Cellulose (2020) 27:8329–8339
https://doi.org/10.1007/s10570-020-03334-z

ORIGINAL RESEARCH

A thermosensitive textile-based drug delivery system for treating UVB-induced damage

Xiao-Zhu Sun · Na Wang

Received: 22 October 2019 / Accepted: 4 July 2020 / Published online: 11 July 2020

Abstract Ultraviolet radiation is one of the most dangerous sources of damage to skin and causes sunburn, erythema, photoaging, and photocarcinogenesis. Some passive drug delivery systems (DDSs) have been developed to treat skin damage. Nevertheless, there have been few studies on the application of intelligent DDSs to enhance the treatment of sunburn. In this paper, thermosensitive microgels were prepared by porous $CaCO_3$ infiltrated by a thermoresponsive polymer, which was synthesized by grafting carboxyl-terminated poly (*N*-vinylcaprolactam) (PVCL-COOH) onto hydrolyzed chitosan. By means of the pad-dry-cure method, microgels were attached to cotton fabrics to develop a medical textile for drug delivery. The results indicated that the microgels were deposited both on the fiber surface and in the space between the fibers. The loaded drug presented a thermoresponsive release profile, and the release mechanism also varied with temperature. After being treated with the medical textile, human keratinocyte HaCaT cells could be protected by inhibiting UVB-induced lactate dehydrogenase leakage and increasing the levels of superoxide dismutase and glutathione peroxidase (GSH-Px). Our study suggested that this thermosensitive microgel-finished cotton fabric can be used as an effective device for the treatment of UVB-induced damage.

X.-Z. Sun (✉)
Institute of Petrochemical Technology, Jilin Institute of Chemical Technology, Jilin 132022, People's Republic of China
e-mail: 329657740@qq.com

N. Wang
ENO Biotechnology Co. Ltd, Dalian 116034, People's Republic of China

Graphic abstract

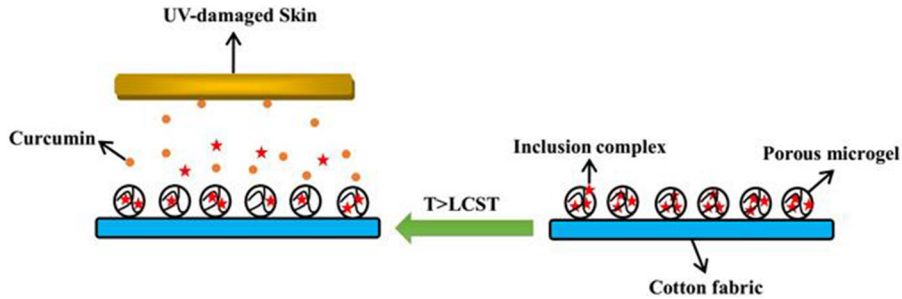

Keywords Thermosensitive · Porous microgel · Drug-releasing textiles · UVB-induced damage

Introduction

The skin is the largest organ of the body, and it protects us from infection and allergy induced by pathogens and small particles. Skin aging is a complicated process and may be influenced by many factors. The most important factor is ultraviolet irradiation (Silva et al. 2014). UV light comprises UVA (320–400 nm), UVB (290–320 nm), and UVC (100–280 nm) radiation. Excessive or frequent exposure to ultraviolet radiation, particularly UVB radiation, is regarded as the main reason for most sunburn and skin damage. UVB-induced pain in sunburn tissue is mainly mediated by impairing the oxidant/antioxidant balance, which gives rise to an increase in the cellular levels of reactive oxygen species (ROS) (Fonseca et al. 2009). Apoptosis at high levels promoted by ROS could lead to significant damage to cell structures (Zorov et al. 2000). Under oxidative stress, skin cells generate SOD and GSH-Px to resist ROS-induced damage (Park et al. 2012).

Curcumin (Cur), found in the rhizome of the plant *Curcuma longa*, is a natural yellow-orange polyphenol with a low molecular weight (Castro et al. 2018; Fang et al. 2003). It has been widely used in Chinese medicine and as a protective agent against chronic diseases due to its extensive pharmacological effects, including anti-inflammatory, antimicrobial, and antioxidant effects (Barsela et al. 2010; Huang et al. 2017). However, applications of Cur suffer from low water solubility and sensitivity to alkaline conditions, and a typical method to overcome these drawbacks is to encapsulate Cur in surfactants, proteins, and cyclodextrins (CD) (Adhikary et al. 2010; Aytac et al. 2017; Mohanty et al. 2012; Yoon et al. 2017). More recently, several studies have demonstrated the protective effects of Cur against skin damage induced by UVB irradiation (Gonçalez et al. 2017; Li et al. 2016). The topical application of Cur prior to UV irradiation causes a delay in tumor appearance, multiplicity, and size (Liu et al. 2018). However, the present photoprotective effect was achieved only by passive drug delivery (Belgio et al. , 2018; Hong et al. 2017), and it would be more beneficial if Cur were delivered through the control of signals from sunburn and if the necessary amount of Cur could be modified by stimuli such as temperature.

Poly(*N*-vinylcaprolactam) (PVCL) is a well-known thermosensitive and biocompatible water-soluble polymer that consists of hydrophilic carboxylic groups and repeating units such as cyclic amide (Çavuş et al. 2015; Cortezlemus et al. 2017; Góis et al. 2016). The lower critical solution temperature (LCST) of PVCL was approximately 32 °C due to the overall change in the hydrophilic–hydrophobic balance; hence, PVCL is suitable for drug delivery and other biomedical applications (Özkahraman et al. 2016; Strokov et al. 2019; Wu et al. 2014). PVCL generates a polymeric carboxylic acid under acidic conditions because of its higher resistance to hydrolysis. Only at concentrations below 10 mg/mL is it nontoxic to fibroblasts (Vihola et al. 2005). Moreover, the phase change temperature of PVCL can be adjusted by grafting PVCL onto backbones with different amphiphilicities (Prabaharan et al. 2010; Rejinold et al. 2011). Chitosan is ideal for

conjugation with PVCL through crosslinking of the amino group and the carboxylic group, and it can impart both LCST tunability and biocompatibility (Srivastava et al. 2009; Wang et al. 2016).

Porous microgels prepared from thermosensitive polymers have attracted a considerable amount of attention due to their fast response to external temperature, and they can also be made on a small scale (Si et al. 2015; Wong et al. 2007). Thus, bioactive molecules, such as aloin and coumarin 6, could be loaded and released into the medium under controlled conditions, which makes microgels a desirable drug delivery system (DDS) (Sun et al. 2017). Template synthesis on a sacrificial core for fabricating microgels is of great interest, and porous $CaCO_3$ microparticles have become popular templates due to their easy preparation procedure, biocompatibility, mild removal conditions, and cost-effectiveness (Liu et al. 2015; Yang et al. 2012; Zhu et al. 2013). The inner structure of porous $CaCO_3$ templates could be adjusted by changing the preparation conditions, for instance, using different crystal growth modifiers or choosing appropriate precipitation conditions (Sergeeva et al. 2015).

The ideal DDS should be biocompatible, mechanically strong, economical to fabricate, and easy to sterilize. Drug-releasing textiles offer promising alternatives with the potential to satisfy these requirements. Textile-based drug-loaded bioactive bandages have been very popular and cost-effective for wound care, transdermal delivery, antimicrobial barriers, and ophthalmic drug carrierste (Khan et al. 2014; Parham et al. 2016; Sadeghi-Kiakhani et al. 2018).

Thus, the present study aimed to develop a novel thermosensitive DDS based on textiles to treat UVB-induced skin damage. Porous $CaCO_3$ particles were utilized as a hard template to prepare thermosensitive microgels. The structure, morphology, and responses to stimuli of the microgels were evaluated, and these materials were further fixed onto cotton fabric by the pad-dry-cure process. The Cur/HP-β-CD inclusion complex was loaded into microgel-finished cotton to prepare textile-based DDSs. The thermoresponsive drug release and release kinetics were studied. The effects and mechanism of microgel-finished fabric in the protection of skin against UVB-induced damage were also determined.

Experimental

Materials

Curcumin, hydrolyzed chitosan (HCS, 2000 Da), and silk fibroin (SF) were supplied by Shaanxi Pioneer Biotech. The following chemicals were provided by Sigma Aldrich: 3-mercaptopropionic acid (MPA), 2,2′-N-hydroxy succinimiade (NHS), 2-Hydroxypropyl-β-cyclodextrin (HP-β-CD), $CaCl_2$, azoisobutyronitrile (AIBN), N-vinyl caprolactam (NVCL), 1-ethyl-3-(3-dimethylamino-propyl)carbodiimide (EDC), tripolyphosphate (TPP), 1,2,3,4-butanetetracarboxylic acid (BTCA), phosphotungstic acid, NaH_2PO_2 (SHP), and dimethylsulfoxide (DMSO). Human keratinocyte HaCaT cells were obtained from iCell Biotech. Scoured and bleached cotton fabrics (36 × 24 yarns per cm^2, 118 g/m^2 weight per unit area) were a gift from Dayao Textile. All chemical reagents were of analytical grade and used as supplied.

Preparation of porous $CaCO_3$

$CaCl_2$ (0.75 g) and SF (3 g) were dissolved in 100 mL water. Then, 20 mL NH_4HCO_3 aqueous solution (0.5 M) was added, and the solution was subjected to sonication for 1 min (Sonics Vibra Cell, 20 kHz with a tip probe). The mixture was placed at room temperature for 1 h. After centrifugation, $CaCO_3$ particles were washed with deionized water and dried in an oven (Lab Companion, China) at 60 °C.

Synthesis of thermosensitive microgels

Microgels were prepared based on our previous work (Sun et al. 2017). HCS-*g*-PVCL was synthesized by grafting PVCL-COOH onto HCS with EDC and NHS as the condensing agents. Then, the copolymer was incubated with the dispersion of $CaCO_3$ particles at 30 °C for 30 min. The solvent was evaporated on a rotor evaporator (RV3V, IKA) at 40 °C. The obtained particles were dispersed in the TPP solution to crosslink the copolymer ($m_{copolymer}$:m_{TPP} = 3:1). After washing with water, dried particles were subsequently dispersed in deionized water, and EDTA (0.1 M, pH 7.0) was added to decompose the $CaCO_3$ templates.

Incorporation of microgels into cotton fabric

The microgels were incorporated into cotton fabric using the pad-dry-cure method. Cotton fabrics were immersed in an aqueous solution containing the microgels, BCTA and NaH_2PO_2 ($m_{microgel}$:m_{BTCA}:m_{SHP} = 6:1.8:0.8). Then, the treated fabrics were passed through a two-roll laboratory padder (Yuanmore Instrument, China) with a water pick-up rate of 85%, and this process was repeated twice. Then, the samples were dried at 60 °C for 15 min and cured at 120 °C for 3 min in an electric laboratory oven.

Preparation of the Cur/HP-β-CD inclusion complex

Cur and HP-β-CD in a molar concentration ratio of 1:2 were ground in a mortar for 1 h with 50% (v/v) ethanol. The mixture was washed with methanol three times to remove the free Cur. The inclusion complex was obtained after drying at 45 °C for 24 h.

Loading of inclusion complex

Microgels or microgel-finished cotton were immersed in aqueous complex solution at 25 °C for 12 h. Then, samples were removed and thoroughly washed to remove the molecules adsorbed on the surface.

Drug encapsulation efficiency

The Cur/HP-β-CD inclusion complex (1 mg) or the complex-loaded microgels (5 mg) was dissolved in 50 mL DMSO to extract Cur for the encapsulation efficiency estimation. The samples in DMSO were gently shaken in a shaking incubator (Jintan Instrument, China) for 24 h at room temperature in the dark. The Cur-extracted DMSO solution was centrifuged at 12,000 rpm for 5 min, and the supernatant DMSO solution containing Cur was collected. The Cur concentration was determined at a wavelength of 446 nm by a UV spectrophotometer (Unico Instrument, China). The encapsulation efficiency (EE) of the complex-loaded microgels was calculated according to the following equation:

$$EE = 1 - (A/B)$$

where A is the amount of Cur in the microgels and B is the amount of Cur in the inclusion complex.

In vitro release study

The drug release experiment was performed for both the complex-loaded microgels (50 mg) and the microgel-finished fabric (1 g) at two different temperatures, 25 °C and 40 °C, in 200 mL of the release medium (pH 7.4 PBS with 0.2% (v/v) Tween 80) (Sun et al. 2013). The microgels were freeze-dried in a freeze dryer (TENLIN Instrument, China), and the microgel-finished cotton was dried in an oven. Then, these two samples were immersed in the release medium. The experiment was conducted using a thermostatic shaking incubator. At predetermined time intervals, 5 mL aliquots were withdrawn for sampling and replaced by an equal volume of the release medium to maintain a constant volume. After certification at 12,000 rpm for 5 min, the sample solutions were analyzed at a wavelength of 428 nm to determine the release of Cur. Pulsatile drug release measurements of the microgel-finished fabric were performed at 25 °C and 40 °C under the same conditions as an on–off switching mechanism. The amount of drug released was plotted as the percentage released versus time. All measurements were conducted in triplicate, and the results are reported as the average value ± S.D.

Characterization

Fourier transform infrared (FTIR) spectroscopy was adopted to identify functional groups (Nicolet Instrument, USA). The morphology was analyzed by scanning electron microscopy (SEM) (JEOL, Japan), transmission electron microscopy (TEM) (JEOL, Japan) and confocal laser scanning microscopy (CLSM) (Caikon, China). The phase transition behavior was evaluated by measuring the apparent hydrodynamic diameter at different temperatures using a nanoparticle size and ζ-potential analyzer (Malvern Instrument, UK).

UVB irradiation and drug treatment

The microgel-finished fabric (1 g) was immersed in 20 mL of culture medium (Dulbecco's modified Eagle's medium) and kept in a thermostatic shaking incubator at 25 °C (C_{25}) or 40 °C (C_{40}) for 6 h. Then, the fabric was removed, and the two media (C_{25} and C_{40}) were left at room temperature.

Human keratinocyte HaCaT cells (CRL-2310, iCell Biotech) were grown and maintained in Dulbecco's modified Eagle's medium supplemented with 10% fetal bovine serum, 100 U/mL penicillin and 100 μg/mL streptomycin. The cells were seeded in 96-well plates at a density of 1×10^4/well. Before treatment, the cells were grown to approximately 60% confluence and then treated with C_{25} or C_{40} for 2 h. C_{25}—or C_{40}-treated cells with a thin cover of PBS were exposed to UVB radiation (40 mJ/cm^2) for 5 min at a distance of 20 cm using a UV radiometer (Waldmann, German). Immediately after irradiation, C_{25} or C_{40} was added to displace PBS for a certain period.

Measurement of cell proliferation

Cells were incubated with C_{25} or C_{40} for 4 h and re-incubated in fresh medium for a certain period. At the specified time point, 100 μL medium was removed, and 15 μL 3-(4,5-dimethyl-2-thiazolyl)-2,5-diphenyl-2-H-tetrazolium bromide (MTT, 5 mg/mL) was added to each well. Then, 150 μL DMSO was added to generate the formazan product. The absorbance at 570 nm was recorded with a microplate reader (Thermo Fisher, USA) to identify the converted dye.

Lactate dehydrogenase (LDH) assay

Cells were incubated with C_{25} or C_{40} for 12 h and re-incubated in fresh medium for 12 h to measure LDH release. An LDH assay kit (Jiancheng Biotech, Chin) was used according to the manufacturer's protocol. The absorbance at 450 nm was measured with a microplate reader.

Measurement of total superoxide dismutase (SOD) activity

Cells were incubated with C_{25} or C_{40} for 12 h and re-incubated in fresh medium for 12–36 h. Then, the cells were rinsed twice with PBS and cracked by an ultrasonic cell disruption system (SONICS&MATERIAL, USA) to harvest the supernatants. An SOD assay kit (Jiancheng Biotech, China) was employed to measure the total SOD activity in the cell lysates. The results were expressed based on the protein concentration in the samples.

Measurement of glutathione peroxidase (GSH-Px) levels

GSH-Px levels were evaluated by means of a glutathione peroxidase quantitation kit (Jiancheng Biotech, China). Cell lysates were centrifuged at 8000 rpm for 10 min at 4 °C to obtain the supernatant for GSH-Px level evaluation. The absorbance at 412 nm was recorded, and GSH-Px levels were calculated according to the decrease in glutathione per milliunits of protein.

Statistical analysis

The results were expressed as the mean ± SD. All data were analyzed by one-way or two-way analysis of variance (ANOVA). For statistical analysis, Student's t-test was performed to compare individual treatments to the controls. The differences were considered statistically significant at $P < 0.05$ (Fig. 1).

Results and discussion

FTIR characterization

FTIR spectra of the samples are shown in Fig. 2 to confirm the reaction process. The spectrum of HCS-*g*-PVCL shows not only the characteristic peaks at 1628 cm^{-1} (amide I band), 1425 cm^{-1} (C–N stretching vibration) and 1376 cm^{-1} (CH_2 deformation band)

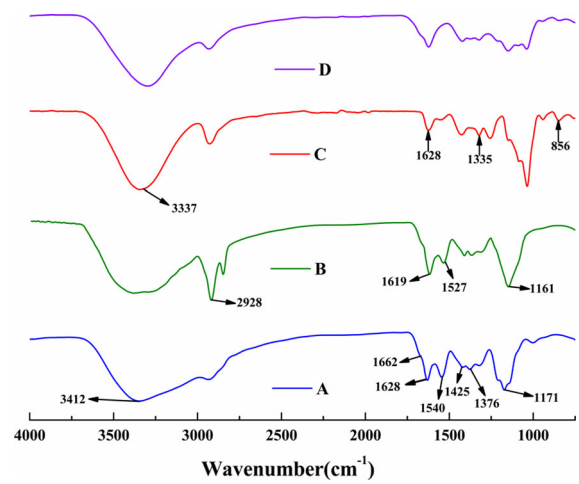

Fig.1 FTIR spectrum of HCS-*g*-PVCL (**a**), a microgel (**b**), an inclusion complex (**c**) and a microgel loaded with complexes (**d**)

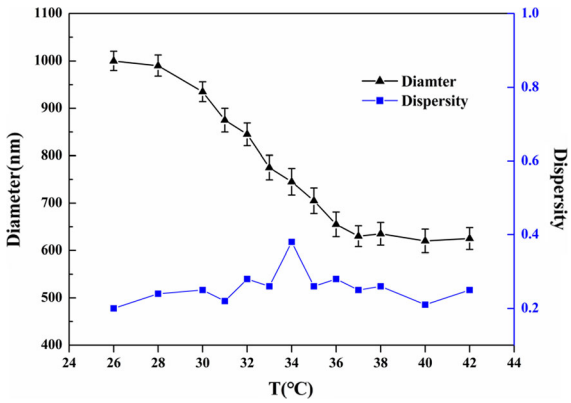

Fig. 2 Particle size and dispersity analysis of microgels during the heating process

corresponding to PVCL but also bands at 3412 cm^{-1} (O–H), 1662 cm^{-1} (amide I band) and 1171 cm^{-1} (C–O stretching vibrations) corresponding to the HCS units. The synthesis of HCS-*g*-PVCL was confirmed by the newly formed amide I band at 1628 cm^{-1} and amide II band at 1540 cm^{-1}. In the microgel spectrum, the characteristic peaks of the amide I band and amide II band shifted to 1619 cm^{-1} and 1527 cm^{-1}, respectively. These changes were attributed to the potential interaction between protonated amine groups and the negative TPP moiety (Rejinold et al. 2011). The peaks attributed to C–O at 1161 cm^{-1} and C-H at 2928 cm^{-1} were enhanced as well. In the spectrum of the complex, several peaks related to HP-β-CD shifted to higher/lower wavenumbers, including 3326 → 3337 cm^{-1}, 1649 → 1628 cm^{-1}, 1362 → 1335 cm^{-1} and 843 → 856 cm^{-1}, demonstrating that Cur was encapsulated in the cavity of HP-β-CD. The spectrum of the microgel-containing complex displayed all the characteristic bands of both the complex and the microgel. These results suggested that the microgels were successfully loaded with the complexes, and the EE was calculated to be 63.4%.

Phase transition studies

The thermoresponsiveness of the microgels was evaluated by determining the apparent hydrodynamic diameter, and the size distribution (dispersity) of the microgels was analyzed by dynamic light scattering (DLS), as depicted in Fig. 2. The dimensions of the microgel decreased considerably when the temperature was increased from 25 °C to 45 °C, and the microgel collapsed to 65% of the original size. Upon the phase transition, water was squeezed out, and the porous microgels became compact. Closure of the pores was another reason for the decrease in particle volume. Furthermore, small dispersity values demonstrated that the microgel particles remained monodisperse during the heating process and shrank uniformly without aggregation. The slight increase in dispersity at 34 °C can be ascribed to the acute phase transition of the copolymer with an LCST of 36 °C. These results suggested that the microgels exhibited good swelling/collapse behavior during the volume phase transition. Furthermore, it was found that the microgels can shrink completely in 8 min. The microgel collapsed faster at a higher temperature.

Morphology

The morphology of $CaCO_3$ in Fig. 3a indicated that the prepared particles treated with SF had a uniform microsphere structure with diameters of approximately 1 μm. The modifying agent SF could not only regulate the formation of microparticles by biomimetic mineralization but also contribute to preserving the biocompatibility of the microspheres (Xiang et al. 2018). More detailed information about the porous $CaCO_3$ particles was obtained by TEM in Fig. 3b. The TEM results indicated that SF and $CaCO_3$ uniformly

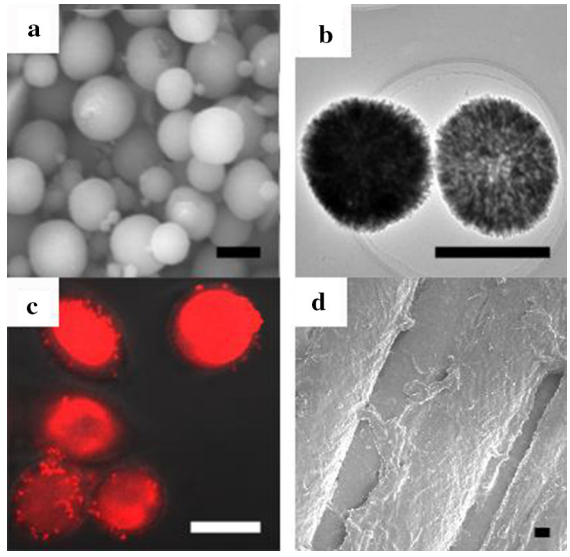

Fig. 3 SEM images of $CaCO_3$ particles (**a**) and microgel-finished cotton (**d**), TEM images of porous $CaCO_3$ (**b**), CLSM images of the microgel (**c**) (Scale bar = 1 μm)

formed inorganic–organic hybrid particles, which may have favored drug loading and sustained release because of the porous and loose structure of the microparticles.

The grafted HCS-*g*-PVCL was loaded inside the pores of $CaCO_3$ to prepare microgels by a solvent evaporation method (Behra et al. 2012). The internal volume of the porous particles was filled by the copolymer molecules, driven by drying and diffusing. TPP was added to produce three-dimensional polymers crosslinked by ionic bonds. Porous thermosensitive microgels were formed, and the $CaCO_3$ templates were removed by EDTA.

A CLSM image of the microgels without the $CaCO_3$ core is shown in Fig. 3c. The size and shape of the microgels after removal of the core are similar to those of the eliminated $CaCO_3$ templates. It can be observed that the microgels had a porous structure applicable for loading/releasing drugs, which demonstrates that the copolymer was homogeneously distributed in the $CaCO_3$ particles (Natalia et al. 2015).

The morphology of the microgel-finished cotton fabric is presented in Fig. 3d. Hydrated microgel particles aggregated after attaching onto the cotton fiber. The shape of the microgels deformed into a pancake structure as a result of water evaporation during drying. In addition, the microgels were deposited not only on the fiber surface but also in the space between the fibers. BTCA was added to crosslink microgels and cotton, which could prevent shedding of the microgels.

In vitro drug release

The in vitro release study of Cur in PBS at varying temperatures is shown in Fig. 4. The amount of drug released was expressed as the percent of drug delivered (M_t) relative to the effective total dose (M_0). From the release profiles, it appeared that more drug was released at 40 °C than at 25 °C for all samples. The microgels released approximately 47% of the total dose in the case of T > LCST in 10 min; in contrast, only 15% of the Cur was released below the LCST. After the initial period, the release rate decreased and almost stabilized, which indicated that swelling equilibrium was achieved. In addition, the microgels showed prominent release compared to the fabric sample because some Cur released from the microgels could be adsorbed onto the cotton surface due to van

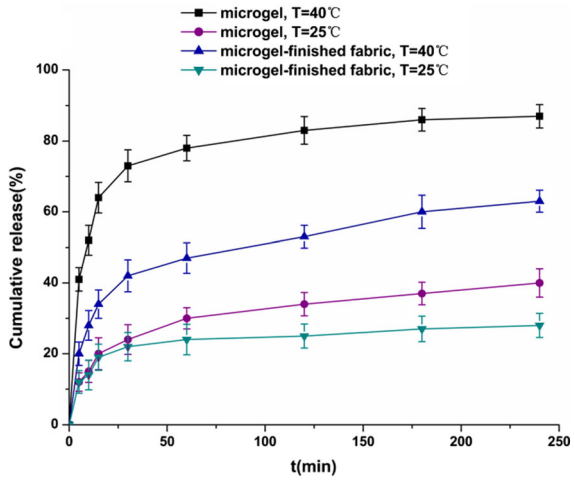

Fig. 4 In vitro temperature drug release profile below (25 °C) and above (40 °C) the LCST

der Waals and hydrogen bond interactions. Moreover, Cur molecules could also enter into the space between the fibers.

The Korsmeyer-Peppas equation ($M_t/M_0 = Kt^n$) was used to analyze the release kinetics (Hayashi et al. 2005). The diffusion index (n) of the samples was calculated to be 0.384 (25 °C, microgel), 0.328 (25 °C, fabric), 0.726 (40 °C, microgel) and 0.765 (40 °C, fabric). When $n < 0.45$, the release of the drug was primarily controlled by Fick's diffusion, whereas when $0.45 < n < 0.89$, the release was regulated by erosion, permeation, and other mechanisms (Zhi-Peng et al. 2012). Samples at 25 °C followed the same release profiles observed at $n < 0.45$, and thus, the drug release was mainly regulated by diffusion and controlled by the swelling of the microgels. The diffusivity of Cur through the network was determined by Fick's diffusion. When T > LCST, the diffusion index was $0.45 < n < 0.89$; therefore, non-Fick's diffusion accommodates the release process at this stage. At this point, shrinking of the microgels is the dominant factor controlling the release process, resulting in deviation of the release profiles from Fick's diffusion. This release mechanism differs from typical non-Fick diffusion mechanisms, such as erosion.

Additionally, Fig. 5 depicts the temperature-triggered release of the drug from the cotton fabric, which presents a pulsatile release pattern. The release followed an on–off pattern when the temperature changed from above to below the LCST in a given

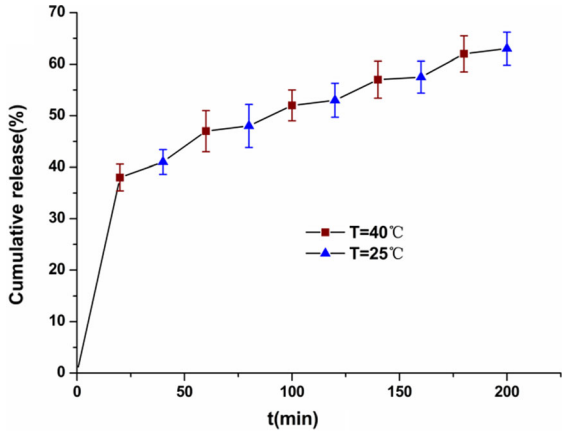

Fig. 5 In vitro pulsatile release profile of microgel-finished fabric below and above the LCST every 20 min

time. These results suggested that the drug release was mainly controlled by shrinkage of the microgels above the LCST, and Cur was removed from the microgels by the released water. The results also confirmed that the concentration gradient controlled the release below the LCST.

Cell proliferation

Cell proliferation of the samples treated under different conditions was assessed using human keratinocytes, as shown in Fig. 6. The results indicated that the HaCaT cell viability and proliferation decreased in a time-dependent manner after UVB irradiation. After UVB irradiation, keratinocyte cell proliferation was suppressed and could be partly improved by the Cur released from the finished fabric from day 1 to day 3. The C_{40} sample contributed more to the recovery of cell activity than C_{25} because more Cur was released at T > LCST. In contrast, there was no significant difference in keratinocyte proliferation for all samples at day 4 and day 5. Chromophore molecules in the skin absorb UV energy to form an excited state, and they undergo a photodynamic reaction through oxidation, which eventually produces ROS by various enzymes and transition metal ions. Some researchers have reported that ROS may cause skin aging and result in intracellular oxidative damage to keratinocytes (Brenneisen et al. 1997; Kozina et al. 2013). These overall observations suggested that microgel-finished fabric could provide protection against UVB-induced ROS overproduction and oxidative damage, which could be realized by the reinforcement of oxidative defense systems, such as SOD and GSH-Px activities.

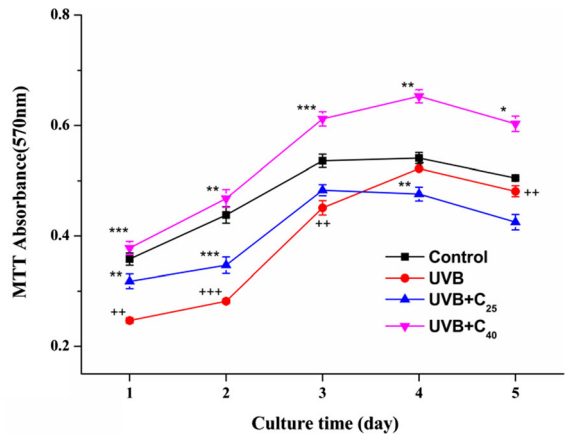

Fig. 6 Cell viability of HaCaT cells exposed to UVB radiation $^{*}P < 0.05$, $^{**}P < 0.01$, $^{***}P < 0.005$ versus the UV irradiation group. $^{+}P < 0.05$, $^{++}P < 0.01$, $^{+++}P < 0.005$ versus the control group

LDH leakage

To further explore the effect of Cur in preventing UVB-induced cytotoxicity in cultured HaCaT cells, we evaluated LDH release from the cytosol to the culture medium, which was used as an index of the loss of membrane integrity. As shown in Fig. 7, UVB irradiation induced a twofold increase in LDH activity, whereas treatment with C_{25} or C_{40} significantly reduced the LDH leakage, indicating that Cur could protect HaCaT against UVB-induced cell damage.

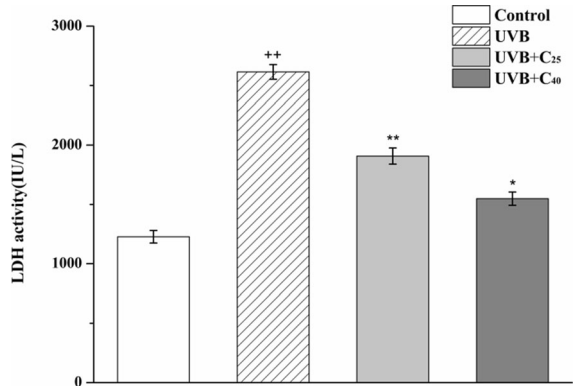

Fig. 7 LDH leakage from HaCaT cells $^{*}P < 0.05$, $^{**}P < 0.01$, $^{***}P < 0.005$ versus the UV irradiation group. $^{+}P < 0.05$, $^{++}P < 0.01$, $^{+++}P < 0.005$ versus the control group

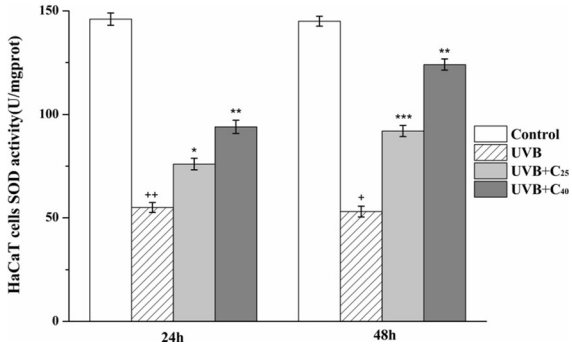

Fig. 8 Total SOD activities in HaCaT cells $^{*}P < 0.05$, $^{**}P < 0.01$, $^{***}P < 0.005$ versus the UV irradiation group. $^{+}P < 0.05$, $^{++}P < 0.01$, $^{+++}P < 0.005$ versus the control group

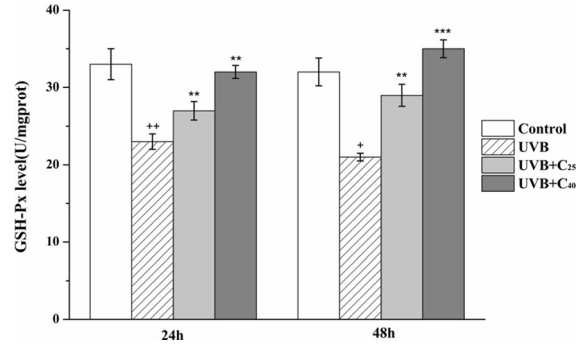

Fig. 9 GSH-Px levels in HaCaT cells $^{*}P < 0.05$, $^{**}P < 0.01$, $^{***}P < 0.005$ versus the UV irradiation group. $^{+}P < 0.05$, $^{++}P < 0.01$, $^{+++}P < 0.005$ versus the control group

HaCaT subjected to UVB irradiation displayed remarkably higher LDH leakage from the cytosol into the culture medium, suggesting a substantial increase in cell membrane permeability. Nevertheless, LDH leakage was inhibited after drug treatment. These results provided evidence that the release of Cur protects HaCaT cells from UVB-induced injury. Notably, C_{40} had a better protective effect on HaCaT against UVB injury because more Cur was released at a higher temperature.

Total SOD activity

To investigate the relationship between UVB-mediated oxidative stress and antioxidant enzymes, we used SOD to measure the antioxidant response of cells, as shown in Fig. 8. Cytosolic SOD activity in HaCaT cells subjected to UVB irradiation at 24–48 h was $62 \pm 3\%$ lower than that in the control group. After treatment with Cur, the HaCaT cells displayed much greater SOD activity than that of the UV-irradiated sample. Therefore, samples treated with C_{40} showed greater enzyme activity in HaCaT cells compared to those treated with C_{25}. It is thought that the cell antioxidative ability via enzymatic activities responded to the generation of ROS. The Cur released from the cotton fabric greatly increased the total SOD activities of the cytosol under UV irradiation, which suggests that ROS production was suppressed. The results implied that keratinocytes could resist UVB-induced damage by inactivating ROS.

GSH-Px Levels

Changes in GSH-Px in the cytoplasm after UVB irradiation were determined to detect whether the UVB stress-regulatory antioxidant enzyme system was accommodated by Cur. As seen in Fig. 9, UVB exposure had a significant effect on the intracellular GSH-Px levels in 48 h compared to that of nonirradiated cells due to inactivation by the increase in ROS or lipid peroxides. After two days, C_{25} or C_{40} treatment effectively increased the GSH-Px levels by $38 \pm 1\%$ and $67 \pm 2\%$, respectively. GSH-Px, mainly located in the cytoplasm and mitochondria, could catalyze the transformation of peroxide to aldehyde and oxidize GSH to GSSH, which would protect the function and structure of the cytomembrane. GSH-Px levels are important biochemical indexes to measure the antioxidant capability of cells. These results indicated that the release of Cur increased the GSH-Px activities inhibited by UVB and protected keratinocytes against UVB-induced oxidative damage.

Conclusions

HCS-*g*-PVCL was synthesized by grafting thermosensitive PVCL-COOH onto HCS. The LCST of the copolymer was larger than that of pure PVCL-COOH due to the hydrophilicity of HCS. Porous microgels were prepared on a $CaCO_3$ hard template using ionic crosslinking. Phase transition studies suggested that the microgels have transition temperatures similar to that of pure HCS-*g*-PVCL. The microgels were then

applied onto cotton fabrics to develop a drug-releasing textile that was used to investigate the release characteristics. When $T > LCST$, more Cur was released at all predetermined time intervals, which was caused by the shrinking and collapse of the microgels. Studies on the kinetics and pulsatile release also confirm this observation. UVB-induced skin cell damage could be avoided by this phenomenon, as confirmed by the decrease in the cell membrane permeability and the increase in the oxidative defense system. These results suggested that this textile-based DDS has the potential to be developed into a flexible smart bandage aimed at limiting UVB-induced cellular oxidative damage and maintaining the integrity of cell membranes.

Acknowledgments The authors acknowledge financial support from The Education Department of Jilin Province (JJKH20190836KJ), Jilin Municipal Education Bureau (201831759), and Jilin Institute of Chemical Technology (2018010).

Author contributions The submission has been received explicitly from all co-authors. And authors whose names appear on the submission have contributed sufficiently to the scientific work and therefore share collective responsibility and accountability for the results

Compliance with ethical standards

Conflict of interest The authors declared that they have no conflicts of interest to this work.

Human and animal rights This article does not contain any studies with human participants or animals performed by any of the authors.

Informed consent Informed consent was obtained from all individual participants included in the study

References

Adhikary R, Carlson PJ, Kee TW et al (2010) Excited-state intramolecular hydrogen atom transfer of curcumin in surfactant micelles. J Phys Chem B 114:2997

Aytac Z, Uyar T (2017) Core-shell nanofibers of curcumin/cyclodextrin inclusion complex and polylactic acid: Enhanced water solubility and slow release of curcumin. Int J Pharm 518:177–184

Barsela G, Epelbaum R, Schaffer M (2010) Curcumin as an anticancer agent: review of the gap between basic and clinical applications. Curr Med Chem 17:190–197

Behra M, Schmidt S, Hartmann J et al (2012) Synthesis of porous PEG microgels using $CaCO_3$ microspheres as hard templates. Macromol Rapid Commun 33:1049–1054

Belgio E, Trsková E, Kotabová E et al (2018) High light acclimation of Chromera velia points to photoprotective NPQ. Photosynth Res 135:263–274

Brenneisen P, Briviba K, Wlaschek M et al (1997) Hydrogen peroxide (H_2O_2) increases the steady-state mRNA levels of collagenase/MMP-1 in human dermal fibroblasts. Free Radic Biol Med 22:515–524

Castro DOD, Tabary N, Martel B et al (2018) Controlled release of carvacrol and curcumin: bio-based food packaging by synergism action of TEMPO-oxidized cellulose nanocrystals and cyclodextrin. Cellulose 25:1249–1263

Çavuş S, Çakal E, Sevgili LM (2015) Solvent dependent swelling behaviour of poly(N -vinylcaprolactam) and poly(N-vinylcaprolactam-co-itaconic acid) gels and determination of solubility parameters. Chem Pap 69:1367–1377

Cortezlemus NA, Liceaclaverie A (2017) Star-shaped copolymers based on poly (N-vinylcaprolactam) and their use as nanocarriers of methotrexate. Aust J Chem 70:1291–1301

Fang JY, Hung CF, Chiu HC et al (2003) Efficacy and irritancy of enhancers on the in-vitro and in-vivo percutaneous absorption of curcumin. J Pharm Pharmacol 55:593–601

Fonseca YM, Catini CD, Vicentini FTMC et al (2009) Protective effect of Calendula officinalis extract against UVB-induced oxidative stress in skin: evaluation of reduced glutathione levels and matrix metalloproteinase secretion. J Ethnopharmacol 127:596–601

Góis JR, Costa JRC, Popov AV et al (2016) Synthesis of well-defined alkyne terminated poly(N-vinyl caprolactam) with stringent control over the LCST by RAFT. Rsc Adv 6:16996–17007

Gonçalez ML, Rigon RB, Pereira-da-Silva MA et al (2017) Curcumin-loaded cationic solid lipid nanoparticles as a potential platform for the treatment of skin disorders. Pharmazie 72:721–727

Hayashi T, Kanbe H, Okada M et al (2005) Formulation study and drug release mechanism of a new theophylline sustained-release preparation. Int J Pharm 304:91–101

Hong YH, Lee HS, Jung EY et al (2017) Photoprotective effects of topical ginseng leaf extract using Ultraflo L against UVB-induced skin damage in hairless mice. J Ginseng Res 41:456–462

Huang B, Liu M, Zhou C (2017) Cellulose–halloysite nanotube composite hydrogels for curcumin delivery. Cellulose 24:2861–2875

Khan MA, Pitcher JD, Kawut SM et al (2014) Bilateral cotton wool spots after use of an endothelin receptor antagonist. Ophthalmic Surg Lasers Imag Retina 45:1–4

Kozina LS, Borzova IV, Arutiunov VA et al (2013) Role of oxidative stress in skin aging. Adv Gerontol 3:18–22

Li H, Gao A, Jiang N et al (2016) Protective effect of curcumin against acute ultraviolet b irradiation induced Photo-damage. Photochem Photobiol 92:808–815

Liu X, She S, Tong W et al (2015) Preparation of elastic polyurethane microcapsules using $CaCO_3$ microparticles as templates for hydrophobic substances loading. RSC Adv 5:5775–5780

Liu X, Zhang R, Shi H et al (2018) Protective effect of curcumin against ultraviolet A irradiation-induced photoaging in human dermal fibroblasts. Mol Med Rep 17:7227–7237

Mohanty C, Das M, Sahoo SK (2012) Emerging role of nanocarriers to increase the solubility and bioavailability of curcumin. Expert Opin Drug Deliv 9:1347–1364

Natalia F, Stoychev G, Puretskiy N et al (2015) Porous thermoresponsive pNIPAM microgels. Eur Polym J 68:650–656

Özkahraman B, Acar I, Gök MK et al (2016) N-vinylcaprolactam-based microgels: synthesis, characterization and drug release applications. Res Chem Intermed 42:6013–6024

Parham S, Chandren S, Wicaksono DHB et al (2016) Textile/Al_2O_3-TiO_2 nanocomposite as an antimicrobial and radical scavenger wound dressing. Rsc Adv 6:8188–8197

Park G, Kim HG, Kim YO et al (2012) Coriandrum sativum L. protects human keratinocytes from oxidative stress by regulating oxidative defense systems. Skin Pharm Phys 25:93–99

Prabaharan M, Grailer JJ, Steeber DA et al (2010) Stimuli-responsive chitosan-graft-poly(N-vinylcaprolactam) as a promising material for controlled hydrophobic drug Delivery. Macromol Biosci 8:843–851

Rejinold NS, Chennazhi KP, Nair SV et al (2011) Biodegradable and thermo-sensitive chitosan-g-poly (N-vinylcaprolactam) nanoparticles as a 5-fluorouracil carrier. Carbohyd Polym 83:776–786

Sadeghi-Kiakhani M, Tehrani-Bagha AR, Safapour S (2018) Enhanced anti-microbial, anti-creasing and dye absorption properties of cotton fabric treated with chitosan-cyanuric chloride hybrid. Cellulose 25:883–893

Sergeeva A, Feoktistova N, Prokopovic V et al (2015) Design of porous alginate hydrogels by sacrificial $CaCO_3$ templates: pore formation mechanism. Adv Mater Interfaces 2:1500386

Si P, Torres JMGT, Hoare T et al (2015) Transmission behavior of pNIPAM microgel particles through porous membranes. J Membr Sci 479:141–147

Silva MA, Trevisan G, Hoffmeister C et al (2014) Anti-inflammatory and antioxidant effects of Aloe saponaria Haw in a model of UVB-induced paw sunburn in rats. J Photochem Photobiol, B 133C:47–54

Srivastava A, Kumar A (2009) Synthesis and characterization of a temperature-responsive biocompatible poly(N-vinylcaprolactam) cryogel: a step towards designing a novel cell scaffold. J Biomater Sci Polym Ed 20:1393–1415

Strokov IV, Abramchuk SS, Makhaeva EE (2019) Salt and pH effect on thermoresponsive behavior of multiwalled carbon nanotube (MWCNT)/poly (N-vinylcaprolactam) dispersion. Colloid Polym Sci 297:387–395

Sun XZ, Williams GR, Hou XX et al (2013) Electrospun curcumin-loaded fibers with potential biomedical applications. Carbohyd Polym 94:147–153

Sun XZ, Wang X, Wu JZ et al (2017) Development of thermosensitive microgel-loaded cotton fabric for controlled drug release. Appl Surf Sci 403:509–518

Vihola H, Laukkanen A, Valtola L et al (2005) Cytotoxicity of thermosensitive polymers poly(N-isopropylacrylamide), poly(N-vinylcaprolactam) and amphiphilically modified poly(N-vinylcaprolactam). Biomaterials 26:3055–3064

Wang Y, Jie W, Han H et al (2016) Self-assembled micelles of N-phthaloylchitosan-g-poly(N-vinylcaprolactam) for temperature-triggered non-steroidal anti-inflammatory drug delivery. J Mater Sci 51:1591–1599

Wong JE, Müller CB, Laschewsky A et al (2007) Direct evidence of layer-by-layer assembly of polyelectrolyte multilayers on soft and porous temperature-sensitive PNiPAM microgel using fluorescence correlation spectroscopy. J Phys Chem B 111:8527–8531

Wu Q, Wang L, Fu X et al (2014) Synthesis and self-assembly of a new amphiphilic thermosensitive poly(N-vinylcaprolactam)/poly(ε-caprolactone) block copolymer. Polym Bull 71:1–18

Xiang Y, Han J, Zhang G et al (2018) Efficient synthesis of starch-regulated porous calcium carbonate microspheres as a carrier for slow-release herbicide. ACS Sust Chem Eng 6:3649–3658

Yang G, Han H, Tingting LI et al (2012) Synthesis of nitrogen-doped porous graphitic carbons using nano-$CaCO_3$ as template, graphitization catalyst, and activating agent. Carbon 50:3753–3765

Yoon SJ, Hyun H, Lee DW et al (2017) Visible light-cured glycol chitosan hydrogel containing a beta-cyclodextrin-curcumin inclusion complex improves wound healing in vivo. Molecules 22:1513

Zhi-Peng C, Wen L, Dan L et al (2012) Development of brucine-loaded microsphere/thermally responsive hydrogel combination system for intra-articular administration. J Control Release 162:628–635

Zhu C, Saito G, Akiyama T (2013) A new $CaCO_3$-template method to synthesize nanoporous manganese oxide hollow structures and their transformation to high-performance $LiMn_2O_4$ cathodes for lithium-ion batteries. J Mater Chem A 1:7077–7082

Zorov DB, Filburn CR, Klotz LO et al (2000) Reactive oxygen species (Ros-Induced) ros release. J Exp Med 192:1001–1014